Journal of Alloys and Compounds 820 (2020) 153415

Contents lists available at ScienceDirect

Journal of Alloys and Compounds

journal homepage: http://www.elsevier.com/locate/jalcom

AlGaN-based UV-C distributed Bragg reflector with a λ-cavity designed for an external cavity structure electron-beam-pumped VCSEL

Y.R. Chen, Z.W. Zhang, G.Q. Miao, H. Jiang, Z.M. Li, H. Song*

State Key Laboratory of Luminescence and Applications, Changchun Institute of Optics, Fine Mechanics and Physics, Chinese Academy of Sciences, Changchun, 130033, PR China

ARTICLE INFO

Article history:
Received 12 August 2019
Received in revised form
12 December 2019
Accepted 16 December 2019
Available online xxx

Keywords:
Distributed Bragg reflector
External cavity structure
III-Nitride semiconductor
UV-C band
AlGaN/AlN superlattices
Electron-beam pumped

ABSTRACT

The external cavity structure electron-beam-pumped (EB-pumped) vertical cavity surface emitting laser (VCSEL) has an important demand for the distributed Bragg reflector (DBR) with an emission window at the working wavelength called λ-cavity. Herein, AlGaN-based UV-C band DBRs with λ-cavities around 280 nm are designed and investigated in detail, which have almost no been reported so far. The DBRs based on alternate stacked $Al_{0.47}Ga_{0.53}N$/AlN bilayers are *in-situ* grown by low-pressure metal-organic chemical vapor deposition (LP-MOCVD). Through a comprehensive protocol of structure optimization by theoretical simulation, epitaxial growth and in-depth characterization and analysis, a high-performance UV-C band DBR with a λ-cavity around 280 nm is successfully fabricated. The DBR presents a reflectivity as high as 81.3% at the λ-cavity, a maximum reflectivity of 89.8% at 282 nm and a stopband with a full-width at half-maximum (FWHM) of 24.7 nm, laying a foundation for developing the external cavity structure EB-pumped AlGaN-based UV-C VCSELs emerging as a promising alternative to the electrically pumped AlGaN-based UV-C lasers.

1. Introduction

So far, the emission wavelength of the practical semiconductor lasers has completely covered the full visible spectrum, and the quantum cascade lasers based on the principles of electrons conducting intersubband transition in the quantum wells and the phonon-assisted resonant tunneling have also expanded the achievable wavelength range to the infrared and the terahertz regimes [1–3]. However, as the application field expands rapidly nowadays, it is of great urgency to develop the short-wavelength semiconductor lasers, especially the UV-C band semiconductor lasers. The reason can be ascribed to their broad application prospects and a huge market demand in both military and civilian fields, such as free-space confidential optical communication, laser lighting, new-generation ultra-high-density optical storage, fine micromaching, high-resolution spectral analysis, biomedical diagnosis, scientific research and so on [4–7].

The wide direct bandgap semiconductor materials are considered as the core materials for the preparation of UV-C lasers. Among them, group-III nitride semiconductors are widely concerned not only because they have stable physical and chemical properties, high intersubband transition probability, but also because they have relatively large exciton binding energy and large exciton recombination probability that make excitons in the semiconductors have strong luminescent transition even at room temperature [8]. Recent breakthroughs mainly include high quality GaN epitaxial growth and its controllable conductive type, which promote the development of group-III nitride semiconductor optoelectronic devices, especially in the fields of high-power light-emitting diodes (LEDs) [9–13] and laser diodes (LDs) [14–16]. However, the wavelength of the electrically pumped LDs based on group-III nitride semiconductors maturely developed and widely used nowadays mainly involves in the blue and near-ultraviolet spectral ranges [17–19]. In fact, it is well known that in order to realize UV-C lasing, the bandgap of the semiconductor must meet the requirements. Fortunately, as one of the most important members of group-III nitride semiconductor family, the bandgap of the ternary alloy AlGaN material can be continuously tuned from 3.4 eV of GaN to 6.2 eV of AlN [20] by adjusting the composition of the aluminum, and the emission wavelength covers the spectral

* Corresponding author.
E-mail address: songh@ciomp.ac.cn (H. Song).

https://doi.org/10.1016/j.jallcom.2019.153415
0925-8388/

range between 365 nm and 200 nm. When the composition of aluminum in AlGaN is higher than 45%, its bandgap will meet the UV-C band. Therefore, AlGaN has become a promising choice for the development of UV-C lasers.

Unfortunately, there are two major reasons that restrict the development of electrically pumped AlGaN-based UV-C lasers. One arises from the poor internal quantum efficiency (IQE). High-density dislocations ($>10^9/cm^2$) are produced in high Al component AlGaN materials prepared by heteroepitaxy due to the lattice mismatch, which act as nonradiative recombination centers in the AlGaN-based optoelectronic devices, thus inhibiting their IQE [21–23]. The other is the low carrier injection efficiency (CIE) caused by the low hole concentration in p-type AlGaN, which directly degrades the hole-related transport property. Generally, the wider the bandgap of AlGaN is, the deeper the activation energy of acceptor becomes [24], which has been confirmed in Mg-doped GaN (160 meV) and AlN (510 meV) [25,26]. As a result, only low hole concentration can be obtained in high Al component AlGaN even if the concentration of magnesium acceptor is high enough, viz., the p-type doping in high Al component AlGaN has always been the technical bottleneck for the development of electrically pumped AlGaN-based UV-C lasers.

Differing from the electrically pumped structure, the electron-beam (EB) pumping method using a structure similar to a field emission display is proposed as a promising alternative [24,27], which is unrestrained by the p-n junction. The active layer so-called the pumping target can be a single semiconductor layer or a low-dimensional structure material such as multiple quantum wells (MQWs) and superlattices (SLs). To date, it has been successfully applied to UV-C light emitting. Oto et al. have realized a light output power of 100 mW and a power efficiency of ~40% at ~240 nm from $Al_{0.69}Ga_{0.31}N$/AlN MQWs pumped by EB [24]. Fukuyo and his colleagues have obtained EB-pumped deep-UV light emission from Si-doped AlGaN MQWs, and an output power of over 15 mW at 256 nm, corresponding to a conversion efficiency over 0.75% was achieved [28]. Tabataba-Vakili et al. have used the pulsed EB with energy of 12 keV and current of 4.4 mA to excite AlGaN-based MQWs and realized a peak optical output power of over 200 mW at 246 nm [29]. Jmerik et al. have reported EB-pumped 235 nm ultraviolet emitters based on ultra-thin GaN/AlN MQWs and achieved a maximum efficiency of 0.75% [30]. The great progress of EB-pumped AlGaN-based UV-C light source not only proves that EB-pumping method is an effective way to get rid of the technical bottleneck made by p-AlGaN, but also provides an important reference for the research on EB-pumped AlGaN-based UV-C laser. Although the crystal quality of the AlGaN-based semiconductor as the pumping target has been improved dramatically by means of modified migration-enhanced epitaxy (MEE), enabling the IQE at room temperature to reach up to 70% at 280 nm [31] and 50% at 250 nm [32], there are still limited reports on the EB-pumped AlGaN-based UV-C VCSELs. Even the most recently reported EB-pumped short-wavelength lasers are only in the UV-A region [33,34]. The issue can be ascribed to the lack of UV-C band optical resonator suitable for the EB-pumping structure, which confines the light to a certain volume through resonant recirculation so as to achieve wavelength selectivity and energy enhancement.

As to the EB-pumping structure, an electron beam source is configured to generate the electron beam incident to the deep-ultraviolet (DUV) MQWs active region grown on the AlN layer by heteroepitaxy. In order to construct a current path between the electron beam source and the active region and avoid charge accumulation, an electrical contact layer must be deposited on the surface of the active region. In this case, the external cavity structure (as shown in Fig. S1 in Supporting Information) is the best choice for the optical resonator, as demonstrated by Wunderer et al. [35]. In our proposed structure, the external reflector (the first reflector) can be a full-reflection dielectric DBR with a reflectivity exceeding 99% in the UV-C band. It is easily obtained from alternate stacked high- and low-refractive index dielectric materials, such as fluorides (LaF_3/AlF_3 or LaF_3/MgF_2) and oxides (Al_2O_3/SiO_2 or HfO_2/SiO_2) [36,37]. The DUV MQWs active region is spaced apart from the first reflector by an external cavity and is adjacent to the second reflector, which is a partial-reflection reflector with an emission window at the working wavelength, so called λ-cavity or cavity mode. As a critical component in constructing the optical resonator, the most effective solution is that a DBR based on AlGaN-based semiconductors *in-situ* grown on the side of the active region serves as the second reflector. However, its development is mainly confined to the visible and long-wavelength UV regions [38,39], only a few reports on the high-reflectivity DBRs in the UV-C region [40–45]. So far, almost no AlGaN-based UV-C DBR with a λ-cavity has been reported.

Herein, for the bottleneck restricting the development of electrically pumped AlGaN-based UV-C VCSELs, a promising alternative by EB-pumping scheme is proposed. Based on the requirement for a DBR with a λ-cavity in the proposed EB-pumped AlGaN-based UV-C VCSEL, the AlGaN-based UV-C band DBR is designed and studied in detail. The evolutions of the refractive index (n) as a function of the wavelength for both AlN and $Al_{0.47}Ga_{0.53}N$ alloys are demonstrated at first, which provide important parameters for designing and simulating alternate stacked $Al_{0.47}Ga_{0.53}N$/AlN DBRs with λ-cavities around 280 nm. Then, the related $Al_{0.47}Ga_{0.53}N$/AlN DBRs with different cycles are prepared by low-pressure metal-organic chemical vapor deposition (LP-MOCVD). Through the effective combination of theoretical simulation, experimental verification and in-depth characterization and analysis, a high-reflectivity UV-C band $Al_{0.47}Ga_{0.53}N$/AlN DBR with a λ-cavity around 280 nm and a stopband with a full-width at half-maximum (FWHM) of about 24.7 nm is successfully fabricated, laying a foundation for the development of the external cavity structure EB-pumped AlGaN-based UV-C VCSELs.

2. Experimental details

2.1. Epitaxial growth of nitride semiconductors

The epitaxial growth was carried out by LP-MOCVD. The monolayer AlN and AlGaN materials were prepared for measuring the relationships between their refractive index (n) and the wavelength. The monolayer AlN material with a thickness of ~1 μm was grown on 2-inch double-polished c-plane sapphire (DP-sapphire). It was prepared by the method of introducing one cycle of the mesothermal AlN (MT-AlN) interlayer on the basis of the traditional two-step growth process (ref. 22) using trimethylaluminium (TMAl) and ammonia (NH_3) as Al and N precursors and hydrogen (H_2) as the carrier gas. The monolayer AlGaN with a thickness of ~1.5 μm was grown on the AlN/DP-sapphire template by supplying additional trimethylgallium (TMGa) along with the TMAl and NH_3 at 1180 °C and the reactor chamber pressure was 50 mbar. AlGaN/AlN superlattices (SLs) with different cycles were fabricated on the AlN/DP-sapphire templates by periodically switching TMGa source on and off at the same growth condition as the monolayer AlGaN. The thicknesses of AlGaN and AlN in each cycle were controlled to be 38 nm and 19 nm, respectively.

2.2. Characterization and measurement

All of the cross-sectional images were characterized using a scanning electron microscope (SEM, Hitachi S-4800). The 2θ-ω

diffraction patterns and the asymmetrical reciprocal space mapping (RSM) images around the $(10\bar{1}5)$ reflection of the materials were obtained by high-resolution X-ray diffractometer (HRXRD, Bruker D8) with a Cu $K\alpha_1$ radiation ($\lambda = 0.15406$ nm). The refractive index values for monolayer AlN and AlGaN were determined by spectroscopic ellipsometry (SE, Semilab GES5E). Both of the SE experimental data were fitted by CompleteEASE software (J.A. Woollam Co., Inc.) using a parametric semiconductor model to reproduce their optical properties. The PL spectra were characterized by a spectrophotometer equipped with a 50 mW 213-nm-wavelength Nd:YAG deep UV laser as the excitation source. The reflection spectra were measured at room temperature using a UV–Vis–NIR spectrophotometer (Hitachi UH4150) and calculated using a commercial simulator (Macleod) for comparison.

3. Results and discussion

3.1. Characterization and measurement of AlN and AlGaN

Fig. 1 (a) and (b) show the cross-sectional SEM images of the bistratal AlGaN/AlN and monolayer AlN grown on c-plane sapphire substrates by LP-MOCVD. Each corresponding structure is also shown in inset. The growth process is described in the experimental section in detail. Fig. 1 (c) and (d) show the 2θ-ω scanning patterns for both bistratal AlGaN/AlN and monolayer AlN layers by HRXRD. As can be seen in Fig. 1 (c), there is one more peak located at 35.24° in addition to the peak of AlN located at 36° (Fig. 1 (d)), which corresponds to the AlGaN layer, and the Al component of the AlGaN layer can be evaluated to be 0.47 by the joint of the Bragg's law, the Vegard law, and the interplanar spacing equation for hexagonal system given by Refs. [27,46,47].

$$2d_{(hkl)} \cdot sin\theta_{(hkl)} = n\lambda \tag{1}$$

$$1 \Big/ d^2_{(hkl)} = 4\left(h^2 + hk + k^2\right) \Big/ 3a^2 + l^2 \Big/ c^2 \tag{2}$$

$$x = (c_{GaN} - c_{AlGaN}) / (c_{GaN} - c_{AlN}) \tag{3}$$

where λ is on behalf of the wavelength of the Cu $K\alpha_1$ radiation. n is the diffraction order. h, k, and l represent the Miller indices of the diffraction plane. $d_{(hkl)}$ and $\theta_{(hkl)}$ are on behalf of the interplanar spacing and the angle between the incident light and the (hkl) plane, respectively. The a and c are the lattice parameters of the hexagonal system. The x is the Al component of the AlGaN. The c_{AlGaN} is on behalf of the c lattice parameter of AlGaN while c_{GaN} and c_{AlN} represent that of the fully relaxed bulk GaN and AlN, which have been identified as 0.31891 nm and 0.31127 nm, respectively [48].

The evolutions of the refractive index (n) as a function of the wavelength for both monolayer AlN and $Al_{0.47}Ga_{0.53}N$ alloys are determined by spectroscopic ellipsometry based on measuring the variation of the polarization of light upon reflection from the surface and interface of the thin film [49]. In order to accurately extract the refractive index of the $Al_{0.47}Ga_{0.53}N$ layer, the AlN layer beneath is preliminarily studied, and its determined thickness and the refractive index are used for the subsequent characterization of the $Al_{0.47}Ga_{0.53}N$ layer. As can be seen in Fig. 1 (e), the refractive index values of the AlN and $Al_{0.47}Ga_{0.53}N$ layers vs. wavelength are summarized in the range of 260 nm–800 nm. The results show that the refractive indices of the AlN and $Al_{0.47}Ga_{0.53}N$ films increase with the increase of photon energy and decrease with the increase of bandgap due to the increase of Al component. An obvious refractive index peak can be observed in the refractive index spectrum located at around 280 nm, which is caused by the intrinsic absorption of $Al_{0.47}Ga_{0.53}N$, basically in accordance with its bandgap. From Fig. 1 (e), the refractive indices of the AlN and $Al_{0.47}Ga_{0.53}N$ under specific photon energy can be obtained for constructing alternate stacked $Al_{0.47}Ga_{0.53}N$/AlN DBRs.

3.2. Structure design and simulation of the AlGaN-based UV-C DBR

Herein, for the purpose of fabricating a UV-C band DBR with a λ-cavity around 280 nm based on alternate stacked $Al_{0.47}Ga_{0.53}N$/AlN structure, the mean thicknesses (t) of AlN and $Al_{0.47}Ga_{0.53}N$ layers in one period can be estimated by the formula of $t = \lambda/4n$, where λ is the center wavelength of the $Al_{0.47}Ga_{0.53}N$/AlN DBR, and n is the refractive index of AlN or $Al_{0.47}Ga_{0.53}N$ under the center wavelength, which can be acquired from Fig. 1 (e). The refractive indices for AlN and $Al_{0.47}Ga_{0.53}N$ around a center wavelength of 280 nm are measured to be 2.234 and 2.571, respectively. Thus, the theoretical thickness of each $Al_{0.47}Ga_{0.53}N$/AlN bilayer can be calculated as approximately 31/27 nm. The schematic diagram of the $Al_{0.47}Ga_{0.53}N$/AlN DBR grown on top of an AlN template is demonstrated in Fig. 2 (a). Based on the structure, the reflection spectrum is simulated and optimized by the standard transmission matrix method [50] using the measured refractive indices shown in Fig. 1 (e). Fig. 2 (b) and (c) show the simulated reflection spectra for

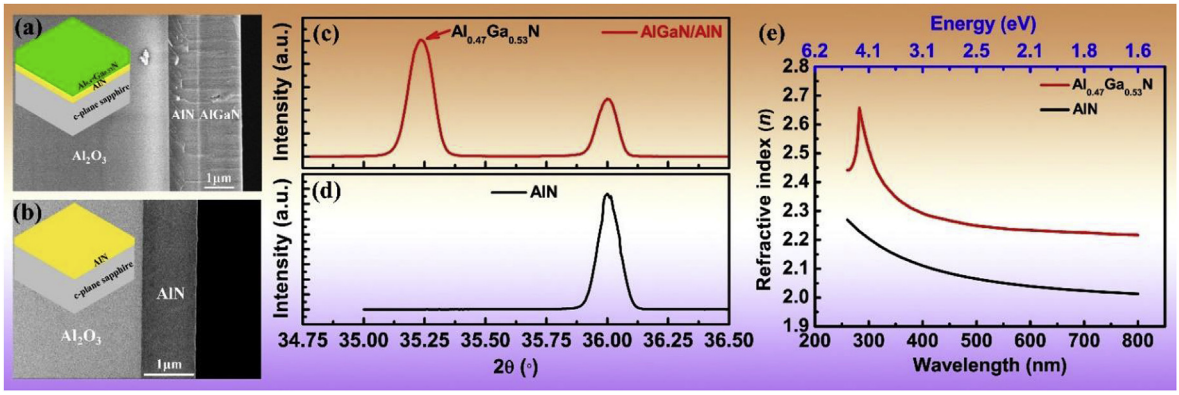

Fig. 1. (a) Cross-sectional SEM image of AlGaN/AlN epilayers grown on a c-plane sapphire substrate. The corresponding structure is shown in inset. (b) Cross-sectional SEM image of an AlN epilayer grown on a c-plane sapphire substrate. The inset shows its structure. (c) and (d) XRD (0002) plane 2θ-ω scanning curves for (a) and (b), respectively. The Al content of AlGaN can be evaluated to be 47%. (e) Evolutions of the refractive index (n) as a function of the wavelength for both AlN and $Al_{0.47}Ga_{0.53}N$ alloys.

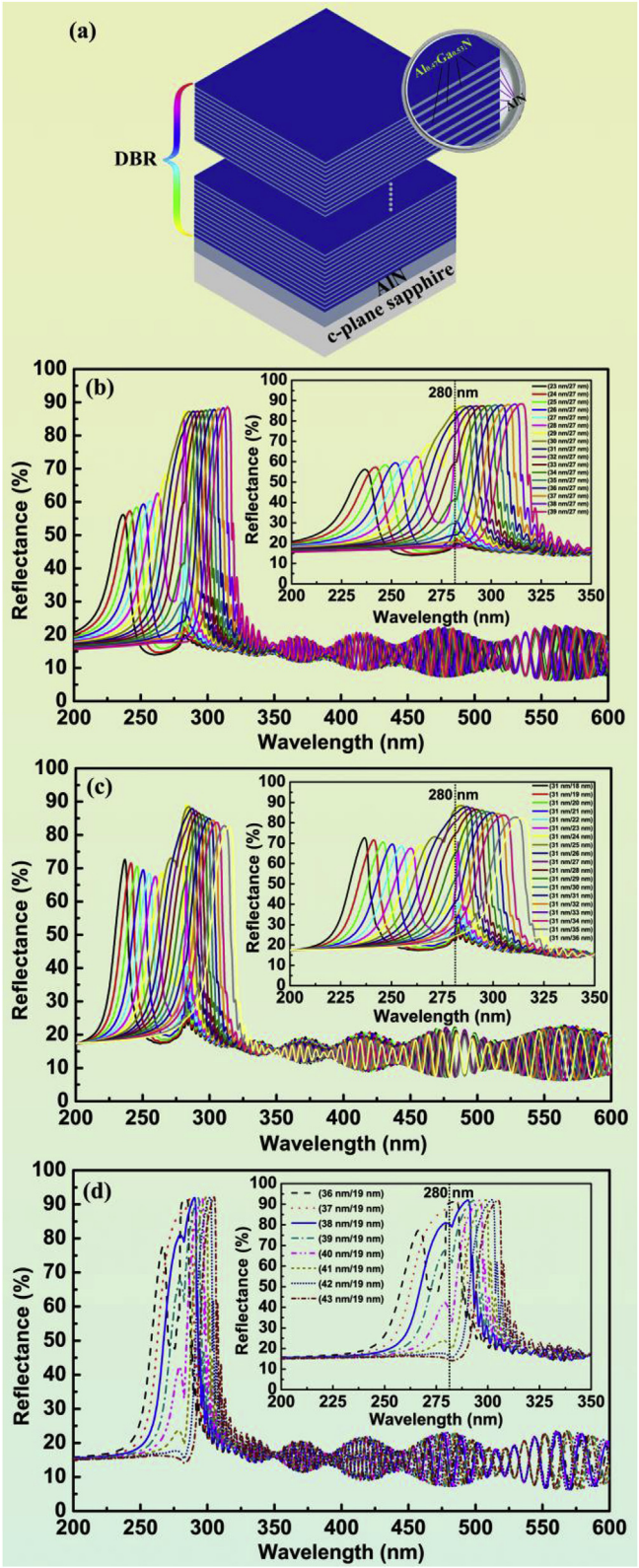

Fig. 2. (a) Schematic diagram of $Al_{0.47}Ga_{0.53}N$/AlN DBR grown on top of an AlN template. Calculated reflection spectra for 59.5 pairs $Al_{0.47}Ga_{0.53}N$/AlN DBR (b) with different thickness of $Al_{0.47}Ga_{0.53}N$ when the thickness of AlN layer is 27 nm, (c) with different thickness of AlN when the thickness of $Al_{0.47}Ga_{0.53}N$ layer is 31 nm, (d) with different thickness of $Al_{0.47}Ga_{0.53}N$ when the thickness of AlN layer is 19 nm.

59.5 pairs $Al_{0.47}Ga_{0.53}N$/AlN DBR on the 1-μm-thick AlN layer with the thickness of $Al_{0.47}Ga_{0.53}N$ layer changing from 23 nm to 39 nm when that of AlN layer is fixed at 27 nm and with the thickness of AlN layer changing from 18 nm to 36 nm when that of $Al_{0.47}Ga_{0.53}N$ layer is fixed at 31 nm, respectively. As can be seen in Fig. 2 (b), to keep the thickness of AlN layers at 27 nm, the thickness of $Al_{0.47}Ga_{0.53}N$ layer is changing around the theoretical value of 31 nm. By increasing the thickness of $Al_{0.47}Ga_{0.53}N$ from 23 nm to 39 nm, the reflection spectrum of the DBR gradually evolves from two discrete reflection peaks to one with an emission window, and finally merges into one reflection peak with a pronounced stopband. In this process, the reflectivity at the center wavelength gradually increases. When the stopband is formed, the center wavelength of DBR has a red shift and deviates from the designed value, though the reflectivity is high. In Fig. 2 (c), the thickness of the $Al_{0.47}Ga_{0.53}N$ layers is kept at 31 nm, the reflectivity of the DBR follows the evolution rule in Fig. 2 (b) when the thickness of AlN changes from 18 nm to 36 nm. The difference lies in the variation trend of the reflectivity intensity. Based on the analysis and a series of simulations, the optimized theoretical thickness for the 59.5 pairs $Al_{0.47}Ga_{0.53}N$/AlN UV-C band DBR with a λ-cavity around 280 nm is obtained in Fig. 2 (d). The optimal thicknesses of AlN and $Al_{0.47}Ga_{0.53}N$ layers are calculated to be 19 nm and 38 nm, respectively, resulting in the formation of a 24-nm-width stopband with a λ-cavity around 280 nm. The reflectivity at 280 nm reaches up to 80%.

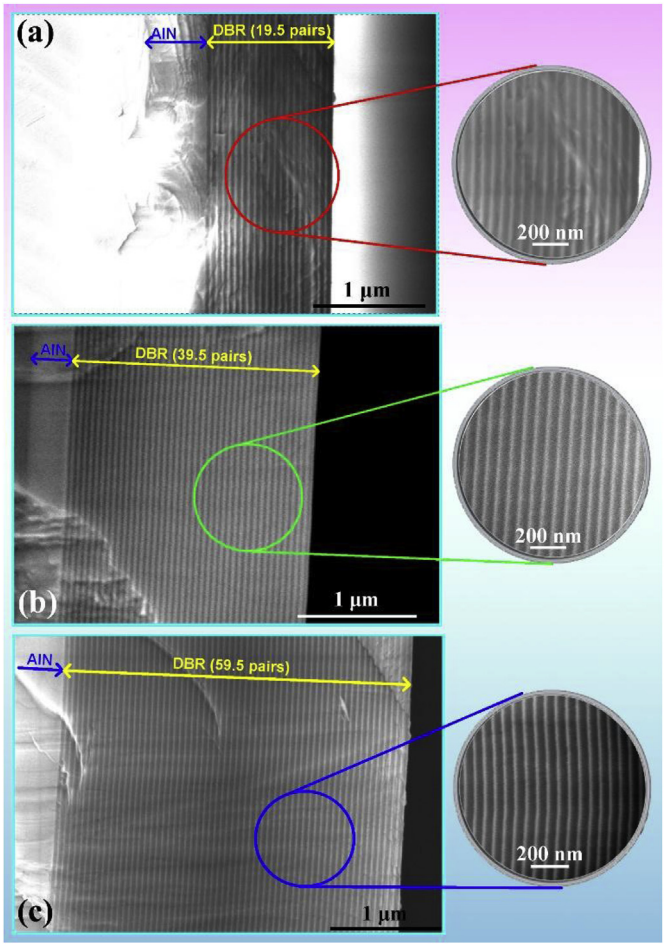

Fig. 3. Cross-sectional SEM images of $Al_{0.47}Ga_{0.53}N$/AlN DBRs with different cycles grown on AlN templates (a) 19.5-pairs, (b) 39.5-pairs, and (c) 59.5-pairs. The partial enlarged images of all samples are shown on the right side of each.

3.3. Characterization and analysis of the AlGaN-based UV-C DBR

On the basis of theoretical optimal calculation, the $Al_{0.47}Ga_{0.53}N$/AlN DBRs with different cycles are grown on the 1-μm-thick AlN templates under the same conditions by controlling the thicknesses of $Al_{0.47}Ga_{0.53}N$ and AlN at about 38 nm and 19 nm, respectively. Fig. 3 shows the cross-sectional SEM images of $Al_{0.47}Ga_{0.53}N$/AlN DBRs with the cycles of 19.5, 39.5 and 59.5, respectively. All samples present a clear and homogeneous layered stack, featuring a constant periodic thickness distribution along the c-axis. The thickness of one cycle $Al_{0.47}Ga_{0.53}N$/AlN roughly estimated from the total thickness of the DBR and the number of cycles and the thickness of $Al_{0.47}Ga_{0.53}N$ (dark streak) almost twice as thick as that of AlN (bright streak) in the partial enlarged images of Fig. 3 can prove the prepared $Al_{0.47}Ga_{0.53}N$/AlN DBR is basically in accordance with the design.

In order to investigate the crystalline quality and the strain evolution of the epitaxial $Al_{0.47}Ga_{0.53}N$/AlN DBRs with different cycles, the 2θ-ω diffraction patterns of the (0002) plane and the asymmetrical RSM images around the $(10\bar{1}5)$ reflection are measured by HRXRD, as shown in Fig. 4 (a)–(d). As seen in Fig. 4 (a), multi-order satellite peaks originated from the periodic bistratal structure are clearly observed in the (0002)-plane 2θ-ω scanning curves of three samples, indicating that the DBRs exhibit good periodicity and clear interfaces, as demonstrated by SEM images. As the number of cycles increases, the number of the satellite peaks increases along both ends of the 2θ-axis. In Fig. 4 (b)–(d), each of the RSMs around $(10\bar{1}5)$ reflection presents a well-resolved main peak which is in accordance with the AlN. The diffraction from the DBR results in a series of satellite peaks along the q_z axis. The axes q_x and q_z represent the directions parallel and perpendicular to the surface of the DBR, which can be used to calculate the in-plane and out-of-plane lattice parameters of the epilayer and thus to evaluate its strain state. From Fig. 4 (b)–(d), the reciprocal lattice points (RLPs), denoted as (q_x, q_z) for the AlN of all three samples are evaluated as (−3.708, 10.037). The uniformity is closely related to their preparation under the same conditions. Since the known RLP for the full relaxed bulk AlN is (−3.71, 10.037) [22], by contrast, the AlN templates used in this paper have little in-plane strain ($\varepsilon_{\parallel}$) that can be neglected and almost have no out-of-plane strain ($\varepsilon_{\perp}$), indicating the high crystalline quality of the AlN templates. It can be said that the DBRs are grown coherently on the almost relaxed AlN templates. In addition, each of the $Al_{0.47}Ga_{0.53}N$/AlN DBRs presents a series of well-resolved sharp satellite peak fringes, further confirming its good periodicity and clear interface. However, the satellite peaks of each sample are distributed along the q_z axis with the same q_x, indicating that the entire DBR structure has the same in-plane lattice parameter. This means that the DBR coherently grows on the AlN template in spite of suffering from the in-plane stress caused by the relatively large lattice mismatch between $Al_{0.47}Ga_{0.53}N$ and AlN. In fact, with the further increase of the periodicity in the $Al_{0.47}Ga_{0.53}N$/AlN DBR, the accumulated in-plane stress will continue to reinforce, and eventually the DBR will release the stress in the manner of cracking. In other words, the

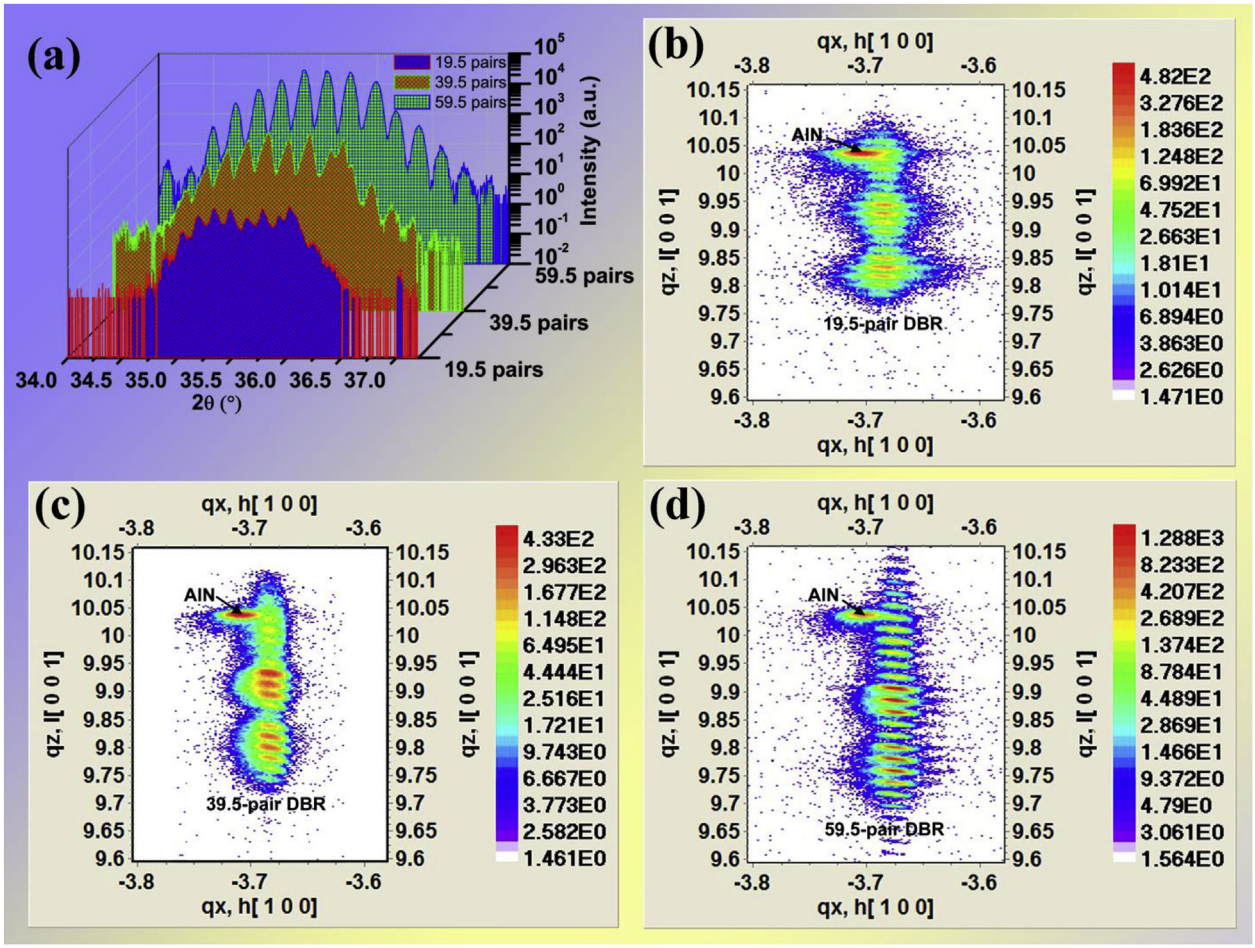

Fig. 4. (a) The 2θ-ω scanning curves of the (0002) plane and (b) the asymmetrical RSMs around the $(10\bar{1}5)$ reflection for $Al_{0.47}Ga_{0.53}N$/AlN DBRs with different cycles.

accumulated in-plane strain impedes the growth of periodic DBR on the AlN template. The limit periodicity for our $Al_{0.47}Ga_{0.53}N$/AlN DBRs grown on the AlN templates is around 59.5 pairs, corresponding to a cracking critical thickness of ~3.4 μm. That is why 59.5 cycles are selected in this paper rather than more. Similar observations have been reported for AlN/$Al_{0.58}Ga_{0.42}N$ DBRs by Moe et al. [51] and for AlN/$Al_{0.65}Ga_{0.35}N$ DBRs by Franke et al. [43] grown on the AlN templates, the former cracked for more than 21 cycles while the later cracked for more than 22 cycles, corresponding to a critical thickness of ~1.3 μm.

The optical properties of the $Al_{0.47}Ga_{0.53}N$/AlN DBRs with different cycles are investigated by room-temperature (RT) PL and reflection spectrum measurements, as shown in Fig. 5. The PL spectra of all DBRs exhibit strong near-band-edge emission of $Al_{0.47}Ga_{0.53}N$ around 280 nm (4.42 eV), as shown in the inset. Another feature of the PL spectra is the long tail emission extending from the near-band-edge located at around 284 nm (4.37 eV). It is caused by the band structure deformation due to the crystal lattice deformation which is originated from the effect of the accumulated in-plane strain in the DBR. The near-band-edge emission and its long tail result in a FWHM of about 9 nm for all PL peaks. It is worth noting that, with the period of the $Al_{0.47}Ga_{0.53}N$/AlN DBR increasing from 19.5 to 59.5, the corresponding near-band-edge emission and its long tail in the PL spectrum occur a slight offset. More specifically, as the number of alternate stacked $Al_{0.47}Ga_{0.53}N$/AlN cycles increases, the near-band-edge emission peak of the DBR has a slight red shift (related variation trend marked by orange dash line) while the long tail has a slight blue offset (marked by green dash line), which can be also ascribed to the effect of the accumulated in-plane strain in the DBR. In Fig. 5, the RT normal incidence reflection spectra for 19.5-pair, 39.5-pair, and 59.5-pair $Al_{0.47}Ga_{0.53}N$/AlN DBRs are presented. The modeled reflection spectrum for 59.5-pair $Al_{0.47}Ga_{0.53}N$/AlN DBR (black dash curve), in accordance with the blue curve in Fig. 2 (d), is provided for comparison. As can be seen, the simulation result is in good agreement with the experimental result for the 59.5-pair DBR. All the experimental reflection spectra consist of a stopband with a λ-cavity located at around 280 nm and clear interference fringes at the low-energy side of the DBR stopband. The absence or inconspicuousness of interference fringes at the high-energy side indicates an obvious fundamental absorption [42]. The reflectivity of the $Al_{0.47}Ga_{0.53}N$/AlN DBR at the λ-cavity improves from 45.6% of the 19.5-pair sample to 81.3% of the 59.5-pair one, and the stopband FWHMs for 19.5-pair, 39.5-pair, and 59.5-pair are about 24.4 nm, 24.6 nm and 24.7 nm, respectively. The maximum reflectivity in the stopband of the three samples is 56.6% at 288 nm, 74.7% at 286 nm, and 89.8% at 282 nm in sequence, indicating that the stopband is slightly shift to the high-energy side when the number of the $Al_{0.47}Ga_{0.53}N$/AlN cycles increases, which can be originated from the accumulated in-plane strain.

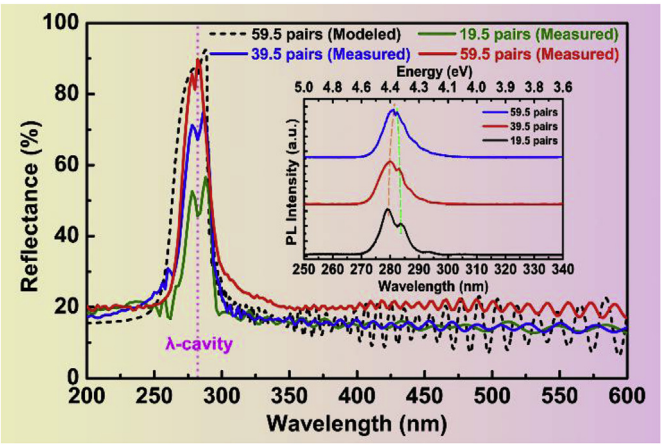

Fig. 5. Experimental reflection spectra for $Al_{0.47}Ga_{0.53}N$/AlN DBRs with different cycles. The black dash curve is the theoretical reflection spectrum of 59.5-pair $Al_{0.47}Ga_{0.53}N$/AlN DBR with the thicknesses of $Al_{0.47}Ga_{0.53}N$ and AlN are 38 nm and 19 nm, respectively. The inset shows the corresponding PL spectra for the $Al_{0.47}Ga_{0.53}N$/AlN DBRs with different cycles.

4. Conclusions

In summary, for the purpose of developing the proposed external cavity structure AlGaN-based UV-C band VCSELs by EB-pumping scheme, it is urgent to design and fabricate high performance UV-C band DBRs with λ-cavities. In this paper, the monolayer AlN and $Al_{0.47}Ga_{0.53}N$ are firstly prepared by LP-MOCVD and their relationships between the refractive index and the wavelength are investigated, which provide important parameters for constructing alternate stacked structure $Al_{0.47}Ga_{0.53}N$/AlN DBRs with λ-cavities around 280 nm. Then, the structural parameters of the $Al_{0.47}Ga_{0.53}N$/AlN DBRs are optimized by theoretical simulation. Based on the optimal parameters, the related $Al_{0.47}Ga_{0.53}N$/AlN DBRs with different cycles are fabricated by LP-MOCVD and carried out detailed characterization and performance analysis. Through the effective combination of theoretical simulation and experimental verification, a 59.5-pair UV-C band $Al_{0.47}Ga_{0.53}N$/AlN DBR with a λ-cavity around 280 nm is successfully developed, which has a reflectivity up to 81.3% at the λ-cavity, a maximum reflectivity of 89.8% at 282 nm and a stopband FWHM of 24.7 nm. This research lays a foundation for the development of the external cavity structure EB-pumped AlGaN-based UV-C band VCSELs.

Author contributions section

Chen Yiren: Conceptualization, Methodology, Data curation, Writing-Original draft preparation, Funding acquisition. **Zhang Zhiwei:** Software, Formal analysis. **Miao Guoqing:** Validation, Resources. **Jiang Hong:** Project administration. **Li Zhiming:** Investigation, Visualization. **Song Hang:** Supervision, Writing-Reviewing and Editing, Funding acquisition.

Declaration of competing interest

The authors declare that they have no known competing financial interests or personal relationships that could have appeared to influence the work reported in this paper.

Acknowledgements

This work was partially supported by the National Natural Science Foundation of China (Grant Nos. 61504144 and 51472230), and the Jilin Provincial Science & Technology Department (Grant No. 20170520156JH).

Appendix A. Supplementary data

Supplementary data to this article can be found online at https://doi.org/10.1016/j.jallcom.2019.153415.

References

[1] C.A. Curwen, J.L. Reno, B.S. Williams, Broadband continuous single-mode tuning of a short-cavity quantum-cascade VECSEL, Nat. Photonics 13 (2019) 855–859.
[2] L. Bosco, M. Franckié, G. Scalari, M. Beck, A. Wacker, J. Faist, Thermoelectrically cooled THz quantum cascade laser operating up to 210 K, Appl. Phys. Lett. 115 (2019), 010601.

[3] Y. Yao, A.J. Hoffman, C.F. Gmachl, Mid-infrared quantum cascade lasers, Nat. Photonics 6 (2012) 432–439.
[4] Z.Y. Xu, B.M. Sadle, Ultraviolet communications: potential and state-of-the-art, IEEE Commun. Mag. 46 (2008) 67–73.
[5] J. Sellés, C. Brimont, G. Cassabois, P. Valvin, T. Guillet, I. Roland, Y. Zeng, X. Checoury, P. Boucaud, M. Mexis, F. Semond, B. Gayral, Deep-UV nitride-on-silicon microdisk lasers, Sci. Rep. 6 (2016) 21650.
[6] M.T. Hardy, D.F. Feezell, S.P. DenBaars, S. Nakamura, Group III-nitride lasers: a materials perspective, Mater. Today 14 (2011) 408–415.
[7] Z. Zhang, M. Kushimoto, T. Sakai, N. Sugiyama, L.J. Schowalter, C. Sasaoka, H. Amano, A 271.8 nm deep-ultraviolet laser diode for room temperature operation, Appl. Phys. Express 12 (2019) 124003.
[8] M. Kneissl, T. Seong, J. Han, H. Amano, The emergence and prospects of deep-ultraviolet light-emitting diode technologies, Nat. Photonics 13 (2019) 233–244.
[9] D.H. Kim, Y.S. Park, D. Kang, K.K. Kim, T.Y. Seong, H. Amano, Combined effects of V pits and chip size on the electrical and optical properties of green InGaN-based light-emitting diodes, J. Alloy. Comp. 796 (2019) 146–152.
[10] E. Matioli, S. Brinkley, K.M. Kelchner, Y.-L. Hu, S. Nakamura, S. DenBaars, J. Speck, C. Weisbuch, High-brightness polarized light-emitting diodes, Light Sci. Appl. 1 (2012) e22.
[11] Y.H. Ra, R. Navamathavan, J.H. Park, C.R. Lee, High-quality uniaxial InxGa1-xN/GaN multiple quantum well (MQW) nanowires (NWs) on Si (111) grown by metal-organic chemical vapor deposition (MOCVD) and light-emitting diode (LED) fabrication, ACS Appl. Mater. Interfaces 5 (2013) 2111–2117.
[12] Y. Li, W.L. Wang, X.C. Li, L.G. Huang, Z.T. Lin, Y.L. Zheng, X.F. Chen, G.Q. Li, Stress and dislocation control of GaN epitaxial films grown on Si substrates and their application in high-performance light-emitting diodes, J. Alloy. Comp. 771 (2019) 1000–1008.
[13] S.H. Lim, Y.H. Ko, C. Rodriguez, S.H. Gong, Y.H. Cho, Electrically driven, phosphor-free, white light-emitting diodes using gallium nitride-based double concentric truncated pyramid structures, Light Sci. Appl. 5 (2016) e16030.
[14] X. Chen, Y. Zhang, J. Yan, Y. Guo, S. Zhang, J. Wang, J. Li, Deep-ultraviolet stimulated emission from AlGaN/AlN multiple-quantum-wells on nano-patterned AlN/sapphire templates with reduced threshold power density, J. Alloy. Comp. 723 (2017) 192–196.
[15] Y. Sun, K. Zhou, M. Feng, Z. Li, Y. Zhou, Q. Sun, J. Liu, L. Zhang, D. Li, X. Sun, D. Li, S. Zhang, M. Ikeda, H. Yang, Room-temperature continuous-wave electrically pumped InGaN/GaN quantum well blue laser diode directly grown on Si, Light Sci. Appl. 7 (2018) e13.
[16] T.J. Slight, S. Watson, S. Viola, A. Yadav, S. Stanczyk, S. Grzanka, S. Gwyn, E. Rafailov, P. Perlin, S.P. Najda, M. Leszczyński, M. Haji, A.E. Kelly, Recent progress in distributed feedback InGaN/GaN laser diodes, Proc. SPIE 10939 (2019) 109390I.
[17] F. Liang, D.G. Zhao, D.S. Jiang, Z.S. Liu, J.J. Zhu, P. Chen, J. Yang, W. Liu, S.T. Liu, Y. Xing, L.Q. Zhang, W.J. Wang, M. Li, Y.T. Zhang, G.T. Du, Improvement of slope efficiency of GaN-based blue laser diodes by using asymmetric MQW and $In_xGa_{1-x}N$ lower waveguide, J. Alloy. Comp. 731 (2018) 243–247.
[18] C. Zhang, R. ElAfandy, J. Han, Distributed Bragg reflectors for GaN-based vertical-cavity surface-emitting lasers, Appl. Sci. 9 (2019) 1593.
[19] B.H. Le, X. Liu, N.H. Tran, S. Zhao, Z. Mi, An electrically injected AlGaN nanowire defect-free photonic crystal ultraviolet laser, Opt. Express 27 (2019) 5843–5850.
[20] P. Tyagi, C. Ramesh, S.S. Kushvaha, M. Mishra, G. Gupta, B.S. Yadav, M.S. Kumar, Dependence of Al incorporation on growth temperature during laser molecular beam epitaxy of $Al_xGa_{1-x}N$ epitaxial layers on sapphire (0001), J. Alloy. Comp. 739 (2018) 122–128.
[21] P. Dong, J. Yan, J. Wang, Y. Zhang, C. Geng, T. Wei, P. Cong, Y. Zhang, J. Zeng, Y. Tian, L. Sun, Q. Yan, J. Li, S. Fan, Z. Qin, 282-nm AlGaN-based deep ultraviolet light-emitting diodes with improved performance on nano-patterned sapphire substrates, Appl. Phys. Lett. 102 (2013) 241113.
[22] Y. Chen, Z. Zhang, H. Jiang, Z. Li, G. Miao, H. Song, The optimized growth of AlN templates for back-illuminated AlGaN-based solar-blind ultraviolet photodetectors by MOCVD, J. Mater. Chem. C 6 (2018) 4936–4942.
[23] T.A. Growden, W. Zhang, E.R. Brown, D.F. Storm, D.J. Meyer, P.R. Berger, Near-UV electroluminescence in unipolar-doped bipolar-tunneling GaN/AlN heterostructures, Light Sci. Appl. 7 (2018) e17150.
[24] T. Oto, R.G. Banal, K. Kataoka, M. Funato, Y. Kawakami, 100 mW deep-ultraviolet emission from aluminium-nitride-based quantum wells pumped by an electron beam, Nat. Photonics 4 (2010) 767–771.
[25] K.B. Nam, M.L. Nakarmi, J. Li, J.Y. Lin, H.X. Jiang, Mg acceptor level in AlN probed by deep ultraviolet photoluminescence, Appl. Phys. Lett. 83 (2003) 878–880.
[26] M. Kneissl, T.Y. Seong, J. Han, H. Amano, The emergence and prospects of deep-ultraviolet light-emitting diode technologies, Nat. Photonics 13 (2019) 233–244.
[27] Y.R. Chen, Z.W. Zhang, H. Jiang, Z.M. Li, G.Q. Miao, H. Song, L.Q. Hu, T.L. Guo, Realization of an efficient electron source by ultraviolet-light-assisted field emission from a one-dimensional ZnO nanorods/n-GaN heterostructure photoconductive detector, Nanoscale 11 (2019) 1351–1359.
[28] F. Fukuyo, S. Ochiai, H. Miyake, K. Hiramatsu, H. Yoshida, Y. Kobayashi, Growth and characterization of AlGaN multiple quantum wells for electron-beam target for deep-ultraviolet light sources, Jpn. J. Appl. Phys. 52 (2013), 01AF03.
[29] F. Tabataba-Vakili, T. Wunderer, M. Kneissl, Z. Yang, M. Teepe, M. Batres, M. Feneberg, B. Vancil, N.M. Johnson, Dominance of radiative recombination from electron-beam-pumped deep-UV AlGaN multi-quantum-well heterostructures, Appl. Phys. Lett. 109 (2016) 181105.
[30] V.N. Jmerik, D.V. Nechaev, A.A. Toropov, E.A. Evropeitsev, V.I. Kozlovsky, V.P. Martovitsky, S. Rouvimov, S.V. Ivanov, High-efficiency electron-beam-pumped sub-240-nm ultraviolet emitters based on ultra-thin GaN/AlN multiple quantum wells grown by plasma-assisted molecular-beam epitaxy on c-Al_2O_3, Appl. Phys. Express 11 (2018), 091003.
[31] M. Shatalov, J. Yang, W. Sun, R. Kennedy, R. Gaska, K. Liu, M. Shur, G. Tamulaitis, Efficiency of light emission in high aluminum content AlGaN quantum wells, J. Appl. Phys. 105 (2009), 073103.
[32] A. Bhattacharyya, T.D. Moustakas, L. Zhou, D.J. Smith, W. Hug, Deep ultraviolet emitting AlGaN quantum wells with high internal quantum efficiency, Appl. Phys. Lett. 94 (2009) 181907.
[33] T. Hayashi, Y. Kawase, N. Nagata, T. Senga, S. Iwayama, M. Iwaya, T. Takeuchi, S. Kamiyama, I. Akasaki, T. Matsumoto, Demonstration of electron beam laser excitation in the UV range using a GaN/AlGaN multiquantum well active layer, Sci. Rep. 7 (2017) 2944.
[34] T. Wunderer, J. Jeschke, Z. Yang, M. Teepe, M. Batres, B. Vancil, N. Johnson, Resonator-length dependence of electron-beam-pumped UV-A GaN-based lasers, IEEE Photonics Technol. Lett. 29 (2017) 1344–1347.
[35] T. Wunderer, N.M. Johnson, M. Park, J.E. Northrup, Electron Beam Pumped Vertical Cavity Surface Emitting Laser, US Patent 10153616 B2 (2018).
[36] J. Sun, X. Li, W. Zhang, K. Yi, J. Shao, High-reflectivity mirrors by Al_2O_3, LaF_3 and AlF_3 for 193 nm application, Opt. Laser. Technol. 56 (2014) 65–70.
[37] M.S. Alias, A.A. Alatawi, W.K. Chong, M. Tangi, J.A. Holguin-Lerma, M.K. Shakfa, T.K. Ng, A.M. Albadri, A.Y. Alyamani, B.S. Ooi, High reflectivity YDH/SiO_2 distributed Bragg reflector for UV-C wavelength regime, IEEE Photonic. J. 10 (2018) 2200508.
[38] C. Berger, A. Dadgar, J. Blasing, A. Krost, In-situ growth monitoring of AlInN/AlGaN distributed Bragg reflectors for the UV-spectral range, J. Cryst. Growth 370 (2013) 87–91.
[39] Y. Liu, S. Wang, H. Xie, T. Kao, K. Mehta, X.J. Jia, S. Shen, P.D. Yoder, F.A. Ponce, T. Detchprohm, R.D. Dupuis, Strain management of AlGaN-based distributed Bragg reflectors with GaN interlayer grown by metalorganic chemical vapor deposition, Appl. Phys. Lett. 109 (2016), 081103.
[40] G. Brummer, D. Nothern, A.Y. Nikiforov, T.D. Moustakas, Deep ultraviolet distributed Bragg reflectors based on graded composition AlGaN alloys, Appl. Phys. Lett. 106 (2015) 221107.
[41] J. Chang, D. Chen, L. Yang, Y. Liu, K. Dong, H. Lu, R. Zhang, Y. Zheng, High-quality crystal growth and characteristics of AlGaN-based solar-blind distributed Bragg reflectors with a tri-layer period structure, Sci. Rep. 6 (2016) 29571.
[42] A. Franke, M.P. Hoffmann, L. Hernandez-Balderrama, F. Kaess, I. Bryan, S. Washiyama, M. Bobea, J. Tweedie, R. Kirste, M. Gerhold, R. Collazo, Z. Sitar, Strain engineered high reflectivity DBRs in the deep UV, Proc. SPIE 9748 (2016) 97481G.
[43] A. Franke, M.P. Hoffmann, R. Kirste, M. Bobea, J. Tweedie, F. Kaess, M. Gerhold, R. Collazo, Z. Sitar, High reflectivity III-nitride UV-C distributed Bragg reflectors for vertical cavity emitting lasers, J. Appl. Phys. 120 (2016) 135703.
[44] A.D. Devine, Simulation, Design, and Fabrication of Deep UV Aluminum Gallium Nitride Distributed Bragg Reflectors, 2018, pp. 30–40 (Chapter 4).
[45] T. Detchprohm, Y. Liu, K. Mehta, S. Wang, H. Xie, T. Kao, S. Shen, P.D. Yoder, F.A. Ponce, Sub 250 nm deep-UV AlGaN/AlN distributed Bragg reflectors, Appl. Phys. Lett. 110 (2017), 011105.
[46] Y.P. Chen, C.H. Zheng, L.Q. Hu, Y.R. Chen, Improved performance of a back-illuminated GaN-based metal-semiconductor-metal ultraviolet photodetector by *in-situ* modification of one-dimensional ZnO nanorods on its screw dislocations, J. Alloy. Comp. 775 (2019) 1213–1220.
[47] A. Aiello, A. Pandey, A. Bhattacharya, J. Gim, X. Liu, D.A. Laleyan, R. Hovden, Z. Mi, P. Bhattacharya, Optical and interface characteristics of $Al_{0.56}Ga_{0.44}N$/$Al_{0.62}Ga_{0.38}N$ multiquantum wells with ~280 nm emission grown by plasma-assisted molecular beam epitaxy, J. Cryst. Growth 508 (2019) 66–71.
[48] D. Wickramaratne, J.X. Shen, C.E. Dreyer, A. Alkauskas, C.G. Van de Walle, Electrical and optical properties of iron in GaN, AlN, and InN, Phys. Rev. B 99 (2019) 205202.
[49] N. Vincent, F. Natali, M. Mihailovic, A. Vasson, J. Leymarie, P. Disseix, D. Byrne, F. Semond, J. Massies, Determination of the refractive indices of AlN, GaN, and $Al_xGa_{1-x}N$ grown on (111) Si substrate, J. Appl. Phys. 93 (2003) 5222–5226.
[50] H.M. Ng, T.D. Moustakas, High reflectivity and broad bandwidth AlN/GaN distributed Bragg reflectors grown by molecular-beam epitaxy, Appl. Phys. Lett. 76 (2000) 2818–2820.
[51] C.G. Moe, Y. Wu, J. Piprek, S. Keller, J.S. Speck, S.P. DenBaars, D. Emerson, AlGaN/AlN distributed Bragg reflectors for deep ultraviolet wavelengths, Phys. Status Solidi A 203 (2006) 1915–1919.